DOI: 10.1002/ ((please add manuscript number))
**Article type: Full Paper**

# Thermally switchable liquid crystals based on cellulose nanocrystals with patchy polymer grafts

*Bailey Risteen, Gwendoline Delepierre, Mohan Srinivasarao, Christoph Weder, Paul Russo, Elsa Reichmanis, Justin Zoppe**

B. Risteen, E. Reichmanis
School of Chemical and Biomolecular Engineering
Georgia Institute of Technology
311 Ferst Dr. NW, Atlanta GA 30332, U.S.A.
E-mail: elsa.reichmanis@chbe.gatech.edu

M. Srinivasarao, P. Russo
School of Materials Science and Engineering
Georgia Institute of Technology
771 Ferst Dr. NW, Atlanta GA 30332, U.S.A.
E-mail: paul.russo@mse.gatech.edu

G. Delepierre, C. Weder, J. Zoppe
Adolphe Merkle Institute
University of Fribourg
Chemin des Verdiers 4, CH-1700 Fribourg, Switzerland
E-mail: justin.zoppe@unifr.ch

Keywords: liquid crystal, cellulose nanocrystals, thermoresponsive, ATRP

A thermally “switchable” liquid-crystalline (LC) phase is observed in aqueous suspensions of rod-shaped cellulose nanocrystals (CNCs) featuring patchy grafts of the thermoresponsive polymer poly(*N*-isopropylacrylamide) (PNIPAM). “Patchy” polymer decoration of the CNCs is achieved by preferential attachment of an ATRP initiator to the ends of the rods and subsequent surface-initiated atom transfer radical polymerization (SI-ATRP). The patchy PNIPAM-grafted CNCs display a higher colloidal stability above the lower critical solution temperature (LCST) of PNIPAM than CNCs that are decorated with PNIPAM in a brush-like manner. A 10 wt% aqueous suspension of the “patchy” PNIPAM-modified CNCs displays

birefringence at room temperature, indicating the presence of a LC phase. When heated above the LCST of PNIPAM (~32 °C), the birefringence disappears, indicating the transition to an isotropic phase. This switching process is fully reversible and appears to be driven by the collapse of the PNIPAM chains above the LCST, causing a reduction of the rods' packing density and thus an increase in translational and rotational freedom. Aqueous suspensions of the "brush" PNIPAM-modified CNCs display a very different behavior. In this case, heating above the LCST causes phase separation while the mesophase is maintained, likely because the chain collapse renders the particles more hydrophobic. The thermal switching observed for the "patchy" PNIPAM-modified CNCs is unprecedented and possibly useful for sensing and smart packaging applications.

## 1. Introduction

Liquid crystals have found widespread technological use in applications ranging from displays[1] to electro-optical devices[2, 3] to lasers.[4, 5] These highly ordered materials are typically formed by the self-assembly of organic molecules or nanoparticles and display anisotropic optical properties, as required by the aforementioned and other applications.[6] The long-range order of liquid crystals makes them also ideal for "templating" other materials such as plasmonic nanoparticles, [7-9] silica, [10-12] and peptides, [13, 14] into complex structures. When templated, these guests can adopt the order and orientation of the liquid-crystalline (LC) host, which can direct chiral assemblies, periodic superstructures, and many other architectures.[15, 16] In this context, aqueous LC suspensions of bio-derived high-aspect-ratio nanoparticles, including cellulose nanocrystals (CNCs) and chitin whiskers, have attracted significant interest in recent years, in part due to the abundance and renewable nature of the respective raw materials, and perhaps also because negative physiological impacts of these nanoparticle types

appear to be modest.[17, 18] Both particle types exhibit LC phases in aqueous suspension and have been used as templates for functional materials.[19-24]

Recently, it was reported that lyotropic CNC suspensions can template the semiconducting polymer poly[3-(potassium-4-butanoate) thiophene-2,5-diyl] (PPBT) into ordered structures in which enhanced π-π interactions between the conjugated macromolecules can be observed.[25] The LC template also showed a moderate response to temperature, which permitted some tunability of the PPBT π-π interactions. While these results show strikingly that CNC-based liquid crystals represent a promising template for organic electronics and other applications, the structural and/or optical response of the lyotropic phase to temperature must be amplified in order to harness the stimuli-responsive behavior.

A widely used approach to impart nanoparticles with temperature-dependent properties is their surface functionalization with a thermoresponsive polymer.[26, 27] The grafting of several thermoresponsive polymers *from* CNC surfaces has been previously achieved via controlled radical polymerization routes after reacting surface hydroxyl groups with suitable initiators, which afforded uniformly decorated "brush"-like modified CNCs.[28-36] In aqueous suspensions, such "hairy" nanoparticles exhibited thermo-reversible aggregation and gelation above the lower critical solution temperature (LCST) of the grafted polymer, resulting in a 4- to 6-fold increase of the hydrodynamic diameter [30, 37, 38] and a corresponding increase of the dynamic storage modulus.[28, 35, 37] Although most of the previous studies have been of fundamental nature, several applications of thermoresponsive-polymer-grafted CNCs have been explored, including Pickering emulsions [39] and triggered drug release.[40] Interestingly, however, little attention has been paid to the details of the self-assembly of such particles, in particular the questions whether or not they form LC phases, and to what extent such LC behavior might be affected by temperature changes around the LCST. In one study, poly(*N*,*N*-dimethylaminoethyl methacrylate) (PDMAEMA)-grafted CNCs were synthesized and the liquid crystal formation

in aqueous suspensions was studied.[41] The hybrid particles formed the same chiral nematic phase as the unmodified CNCs,[42] but above the LCST, the pitch of the chiral nematic twist decreased slightly and phase separation was observed, due to attractive interactions between the rods upon collapse of the PDMAEMA grafts.

Different polymer graft morphologies are possible through "topochemical" or surface-selective functionalization of CNCs. A wide variety of topochemical modifications has been achieved on CNCs through chemistry on the reducing ends of the rods including thiolation,[43, 44] protein immobilization,[45] and polymer grafting.[46, 47] Successful grafting of polymers both *to* and *from* CNCs was first demonstrated by Sipahi-Sağlam *et al*. through hydrazone linkages at the reducing ends.[47] The grafting-*to* chemistry consisted of reacting amino-terminated poly(ethyleneglycol) or poly(dimethylsiloxane) to carboxyl-terminated CNCs, whereas the grafting-*from* approach relied on the selective immobilization of an azo initiator that was used to initiate the radical polymerization of acrylamide. Zoppe *et al*.[46] expanded on this work by introducing a water-tolerant synthetic route to selectively modify CNCs with an alkyl bromide ATRP initiator at the reducing ends; poly(*N*-isopropylacrylamide), poly[2-(methacryloyloxy)ethyltrimethylammonium chloride], and poly(sodium 4-styrenesulfonate) were all successfully grafted from CNCs using this method.

Here, a topochemical route was applied to functionalize CNCs with the thermoresponsive polymer PNIPAM, based on the hypothesis that the thermoresponsive particles thus made should largely retain their electrostatic interactions and high aspect ratio, both of which are important in forming LC phases.[48] Selectively grafted or "patchy" CNCs were produced by growing PNIPAM from initiator sites via surface-initiated atom transfer radical polymerization (SI-ATRP). Indeed, as targeted, the patchy PNIPAM-grafted CNCs displayed a higher colloidal stability in water above the LCST of the grafted PNIPAM (~32 °C [43, 49]) than reference CNCs that were decorated with PNIPAM in a brush-like manner. As a result, the mesophase of the

patchy CNCs could reversibly be switched from a LC to an isotropic state around the LCST. By contrast, heating aqueous suspensions of the "brush" PNIPAM-modified CNCs causes phase separation while the mesophase is maintained.

## 2. Results and Discussion

CNCs derived from wood-pulp were purchased from the USDA Forest Products Laboratory (FPL). A length of 106 ± 39 nm and a width of 11 ± 2.5 nm was measured by AFM (**Figure S1**). CNCs from which PNIPAM was grafted in a "patchy" manner, herein referred to as *p*-PNIPAM-*g*-CNCs, were synthesized by preferentially modifying the particle surface with an ATRP initiator and growing PNIPAM from those sites. For this modification, the aldehyde groups on the reducing ends of the cellulose molecules were oxidized to carboxylic acid groups (**Scheme 1**). The CNCs used in this study (USDA Forest Products Laboratory, Madison, WI) were primarily cellulose II polymorphs, as evidenced by the wide-angle X-ray diffraction pattern (**Figure S2**), which shows characteristic peak maxima at 2θ values of 19.8 ° and 21.8 °, corresponding to the (110) and (020) lattice planes, respectively. A minor component of the CNCs is from the cellulose I polymorph as small characteristic peaks were observed between 14 ° - 17 ° and 34.3 °, corresponding to the $(1\bar{1}0)$, (110) and (040) lattice planes, respectively.[50, 51] Mixtures of two polymorphs for CNCs from the same supplier were reported previously by Reid et al.[52] The source of this thermodynamically more stable cellulose polymorph could either be due to a concentrated NaOH treatment during the production process or it could be present in the starting material. As a result of this morphology, the CNCs used here feature aldehyde groups on both ends. Their concentration was quantified through a bicinchoninic acid (BCA) assay, in which Cu(II) ions are reduced by the aldehyde groups to Cu(I); a purple-colored complex is formed in presence of BCA, which can be quantified by colorimetric

methods.[53, 54] The concentration of reducing end groups in the as-received CNCs was found to be 18.2 µmol CHO/g CNCs. By performing the BCA assay before and after the oxidation of the reducing ends with $NaClO_2$, a yield of 57% was determined for this reaction. The carboxylic acid groups were subsequently reacted with an excess of ethylenediamine (EDA). The concentration of primary amine groups thus introduced was quantified by the ninhydrin (2,2-dihydroxyindane-1,3-dione) assay yielding 60.3 µmol $NH_2$/g CNCs.[55-57] This amine content is higher than what would be expected in the case of quantitative functionalization of the oxidized aldehydes groups and reflects that the unmodified CNCs contain a non-negligible portion of -COOH groups on their surface (ca. 26 µmol COOH/g CNCs, as determined by conductometric titration [58], **Figure S3**), which were also able to react with the ethylenediamine.[58, 59] The source of the COOH groups is unknown but might be present in the starting material or might be due to an oxidation during acid hydrolysis. In addition, some physical adsorption of ethylendiamine on the CNC surfaces, either through hydrogen bonding or electrostatic interactions, may be at play. Thus, while an accurate yield of the amination reaction could not be established, the efficacy was estimated by repeating the ninhydrin assay after attachment of the alkyl bromide initiator to the CNC surface. The value of 5.3 µmol $NH_2$/g CNCs suggests a reaction yield of 91%. Using previously reported conditions, PNIPAM was successfully grown *from* the alkyl bromide initiator sites to yield thermoresponsive CNCs.[46] Given the above analysis, the PNIPAM chains cannot be expected to grow exclusively from the ends of the particles, but a significant fraction should originate from the rest of their surface, rendering the decoration "patchy".

For the purpose of comparison, CNCs were also decorated with PNIPAM in a brush-like manner (**Scheme 2**). This was achieved by Fischer esterification of the primary surface hydroxyl groups with 2-bromopropionic acid to achieve uniform initiator decoration, followed by the polymerization of NIPAM using the same SI-ATRP conditions.[46] This sample is

designated *b*-PNIPAM-*g*-CNCs and was measured to have a Br content of 1.72 wt% or ~215 µmol/g CNCs via elemental analysis. Using this data and assuming that the fraction of surface cellulose chains is 0.19 and that 1.5 surface hydroxyl groups are reactive per anhydroglucose unit, [60, 61] the conversion of the surface OH groups was calculated to be 12.6%. The density of initiator groups was calculated to be 0.517/nm$^2$, using the following equation:

$$(1)\ \sigma = \frac{W N_A}{MW A}$$

where $W$ is the weight fraction of the attached initiator, $N_A$ is Avogadro's constant, $MW$ is the molecular weight of the attached initiator, and $A$ is the surface area of the CNCs (258 m$^2$/g, measured using methods reported previously).[46, 62]

**Scheme 1. "Patchy" SI-ATRP of PNIPAM from CNCs.**

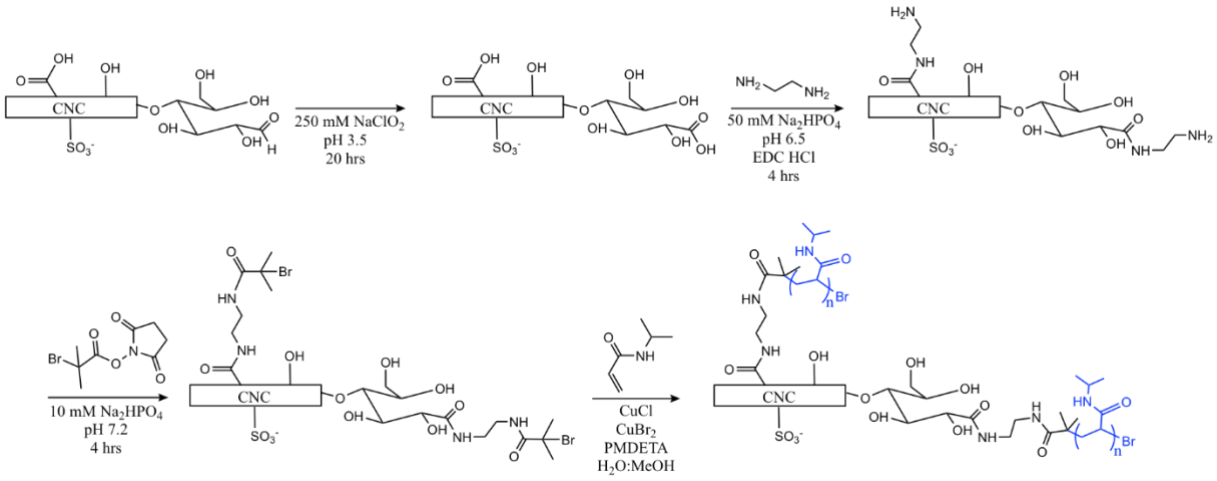


**Scheme 2. "Brush" SI-ATRP of PNIPAM from CNCs.**

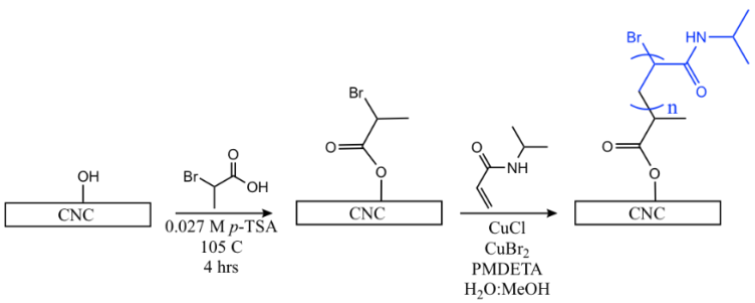

The successful growth of PNIPAM from the CNCs (both "patchy" and "brush" morphologies) was confirmed by FTIR spectroscopy. The amide stretching and bending associated with the PNIPAM appeared in the spectra of the modified CNCs at around 1650 $cm^{-1}$ and 1540 $cm^{-1}$, respectively (**Figure 1**).[28] The vibrational mode associated with the -$CH_3$ group of the isopropyl moiety in PNIPAM was also found around 2970 $cm^{-1}$ in both spectra. As expected, all three of these peaks were more pronounced in the spectrum of *b*-PNIPAM-*g*-CNCs, due to the higher grafting density in this material (*vide infra*).

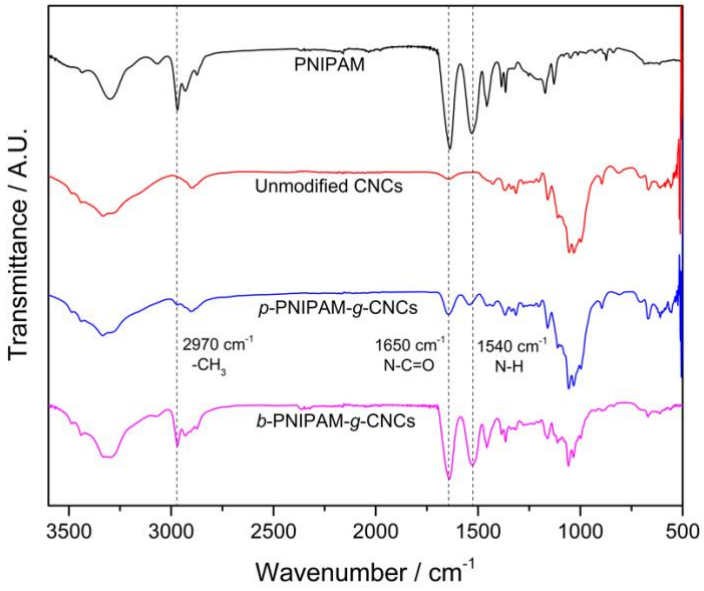


**Figure 1**. FTIR transmittance spectra of PNIPAM, unmodified CNCs, *p*-PNIPAM-*g*-CNCs, and *b*-PNIPAM-*g*-CNCs. Dashed lines at 2970, 1650, and 1540 $cm^{-1}$ highlight the vibrational mode associated with the PNIPAM's -$CH_3$ group, and the polymer's amide stretching and bending.

The amount of grafted PNIPAM was estimated from thermogravimetric analysis (TGA) of the unmodified and modified particles (**Figure 2**). The neat CNCs and *p*-PNIPAM-*g*-CNCs both exhibit an onset of degradation around 275 °C, whereas the *b*-PNIPAM-*g*-CNCs starts to degrade at ~315 °C, *i.e.*, closer to the degradation onset of neat PNIPAM (~350 °C). Due to the covalently attached polymers on the surface of the CNCs, their thermal stability is increased.[46] The first derivative curves of the PNIPAM-modified CNCs show two peaks: the initial

degradation of the cellulose component, followed by the mass loss associated with the PNIPAM starting at 400 °C. A Gaussian peak fitting procedure (**Figure S4**) provided an estimation of the relative contributions and thereby allowed an approximation of the polymer content;[63] the analysis resulted in a PNIPAM content of 18 wt% for *p*-PNIPAM-*g*-CNCs and 37 wt% for the *b*-PNIPAM-*g*-CNCs.

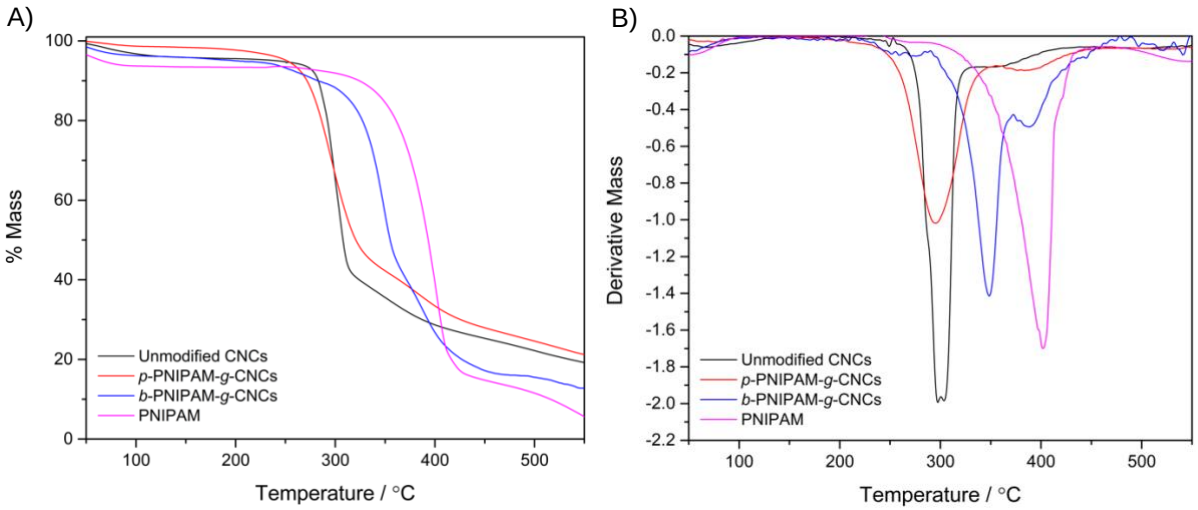


**Figure 2**. (A) Thermogram and (B) 1st derivative curves from TGA of unmodified CNCs, *p*-PNIPAM-*g*-CNCs, *b*-PNIPAM-*g*-CNCs, and PNIPAM.

The polymer grafts were cleaved from the CNCs by alkaline hydrolysis[29] and their molecular weights and dispersities were determined using size exclusion chromatography (SEC). The cleaved PNIPAM from the "patchy" CNCs had a number-average molecular weight ($M_n$) of 60,440 g/mol and a dispersity ($Đ$) of 1.89. The "brush" PNIPAM had an $M_n$ of 134,500 g/mol and a $Đ$ of 1.39 (**Figure 3**). A potential explanation for the higher molecular weight of the PNIPAM chains of the "brush" modified CNCs is the so-called "growing viscous front" effect, observed by Behling *et al.* for SI-ATRP of styrene from clay particles, in which a high local viscosity at the particle interface and low separation of active sites leads to a higher rate of chain propagation at high surface grafting densities.[64] The grafting density for the "brush" CNCs was calculated to be 0.00642 chains/nm$^2$ using Equation 1, where $W$ is the weight of the cleaved polymer and $M_n$ is used instead of $MW$.[62] Thus, the initiator efficiency was 1.24%.

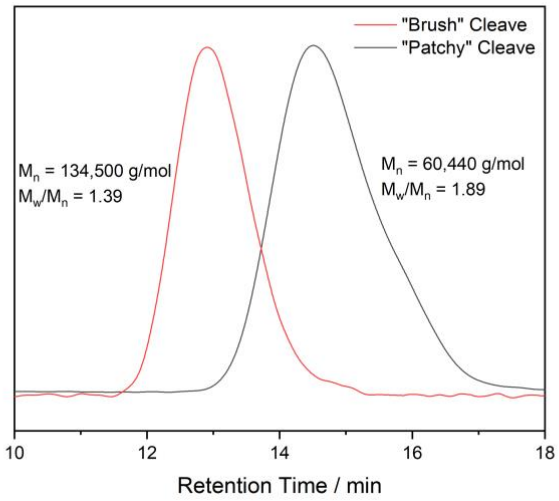


**Figure 3**. SEC curves of PNIPAM cleaved from *p*-PNIPAM-*g*-CNCs ("patchy") and *b*-PNIPAM-*g*-CNCs ("brush").

The greatest difference between the "patchy" and "brush" modified PNIPAM-CNCs was their colloidal stability in water. The *p*-PNIPAM-*g*-CNCs were stable even above the LCST of PNIPAM; the zeta potential of a 0.1 wt% suspension was -34.5 ± 1.0 mV at 25 °C and -36.4 ± 1.3 mV at 40 °C with no visible agglomeration at the higher temperature. The high colloidal stability above the LCST is likely related to the fact that *p*-PNIPAM-*g*-CNCs retained much of their negative charges from sulfate half-ester groups introduced during sulfuric acid hydrolysis used in their isolation from cellulose pulp.[42] The *b*-PNIPAM-*g*-CNCs had a zeta potential of -1.1 ± 0.1 at 25 °C and -2.5 ± 0.2 at 40 °C. The slight increase in the magnitude of the zeta potential with temperature might be associated with the collapse of PNIPAM chains above the LCST, exposing unreacted sulfate half ester groups. Unlike the *p*-PNIPAM-*g*-CNCs, the *b*-PNIPAM-*g*-CNCs aggregated significantly above the LCST as indicated by the fact that the dispersion became turbid (**Figure S5**).

Multi-angle dynamic light scattering (MADLS) was used to measure the average apparent hydrodynamic radius ($R_{h,app}$) of the particles as a function of temperature (**Figure 4**). At room

temperature, the unmodified CNCs had an $R_{h,app}$ of ~80 nm whereas the "patchy" PNIPAM-CNCs and "brush" PNIPAM-CNCs were larger due to the presence of the polymer grafts with $R_{h,app}$ of 106 nm and 144 nm, respectively. When heated above the LCST, the unmodified CNCs did not change size in contrast to both modified particles at 40 °C. At this temperature, the *p*-PNIPAM-*g*-CNCs displayed an $R_{h,app}$ of 137 nm (29% increase), whereas the value of *b*-PNIPAM-*g*-CNCs rose to 3460 nm (2300% increase), indicative of aggregation (**Table 1**). The aggregation of the *b*-PNIPAM-*g*-CNCs was accompanied by a step-wise increase in the static light scattering intensity (**Figure S7**).

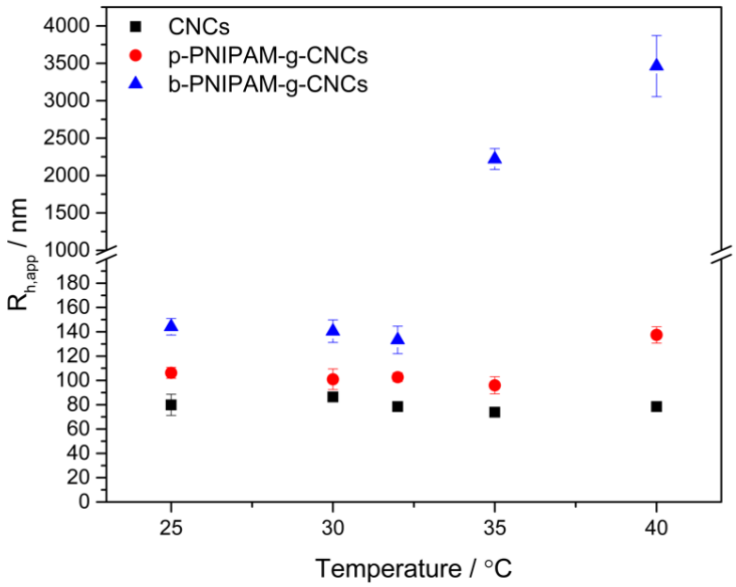


**Figure 4**. Average apparent hydrodynamic radius ($R_{h,app}$) of unmodified CNCs, *p*-PNIPAM-*g*-CNCs, and *b*-PNIPAM-*g*-CNCs as a function of temperature.

**Table 1**. Zeta potential values and apparent hydrodynamic radii ($R_{h,app}$) of unmodified CNCs, *p*-PNIPAM-*g*-CNCs, and *b*-PNIPAM-*g*-CNCs below (25 °C) and above the LCST (40 °C) of PNIPAM.

| | CNCs | | *p*-PNIPAM-*g*-CNCs | | *b*-PNIPAM-*g*-CNCs | |
|---|---|---|---|---|---|---|
| | 25 °C | 40 °C | 25 °C | 40 °C | 25 °C | 40 °C |
| Zeta Potential (mV) | -34.3 ± 2.2 | -33.6 ± 1.2 | -34.5 ± 1.0 | -36.4 ± 1.3 | -1.1 ± 0.1 | -2.5 ± 0.2 |
| $R_{h,app}$ (nm) | 79.9 ± 8.7 | 78.4 ± 2.1 | 106 ± 5 | 137 ± 3 | 144 ± 7 | 3460 ± 410 |

At a total concentration of 10 wt%, aqueous dispersions of the *p*-PNIPAM-*g*-CNCs (corresponding to ~8.2 wt% CNCs and 1.8 wt% PNIPAM grafts based on TGA) displayed birefringence at room temperature, consistent with the formation of a LC phase (**Figure 5a-b**). This concentration was chosen to be in the nematic phase based on phase diagrams of unmodified CNCs.[25] When the sample was heated to 40 °C, the birefringence nearly disappeared, suggesting a change from a LC state towards an isotropic state (Figure 5c-d). The cross-polarized microscopy images do not show the characteristic fingerprint texture of the chiral nematic phase (or cholesteric), as is often observed for CNC suspensions.[65] This cholesteric phase is speculated to be due to the chirality of the crystalline rods themselves [66] and in the case of the modified-CNCs studied here, the PNIPAM grafts may provide steric effects that prevent locally high concentrations of particles. An alternative explanation is that the particle concentrations studied were too low to observe the pitch under the microscope; previous studies have shown that decreasing concentrations of CNCs result in an increase in the pitch.[67] However, samples prepared with 17 wt% CNCs did not show the fingerprint texture either (**Figure S8**). In the case of the *p*-PNIPAM-*g*-CNCs sample, only slight differences were observed when the analyzer was rotated by ± 5º with respect to the polarizer (which should reveal differences in the birefringence for chiral samples, **Figure S9**), whereas a much more pronounced change was seen for a reference suspension containing 8.2 wt% of unmodified CNCs (**Figure S10**).

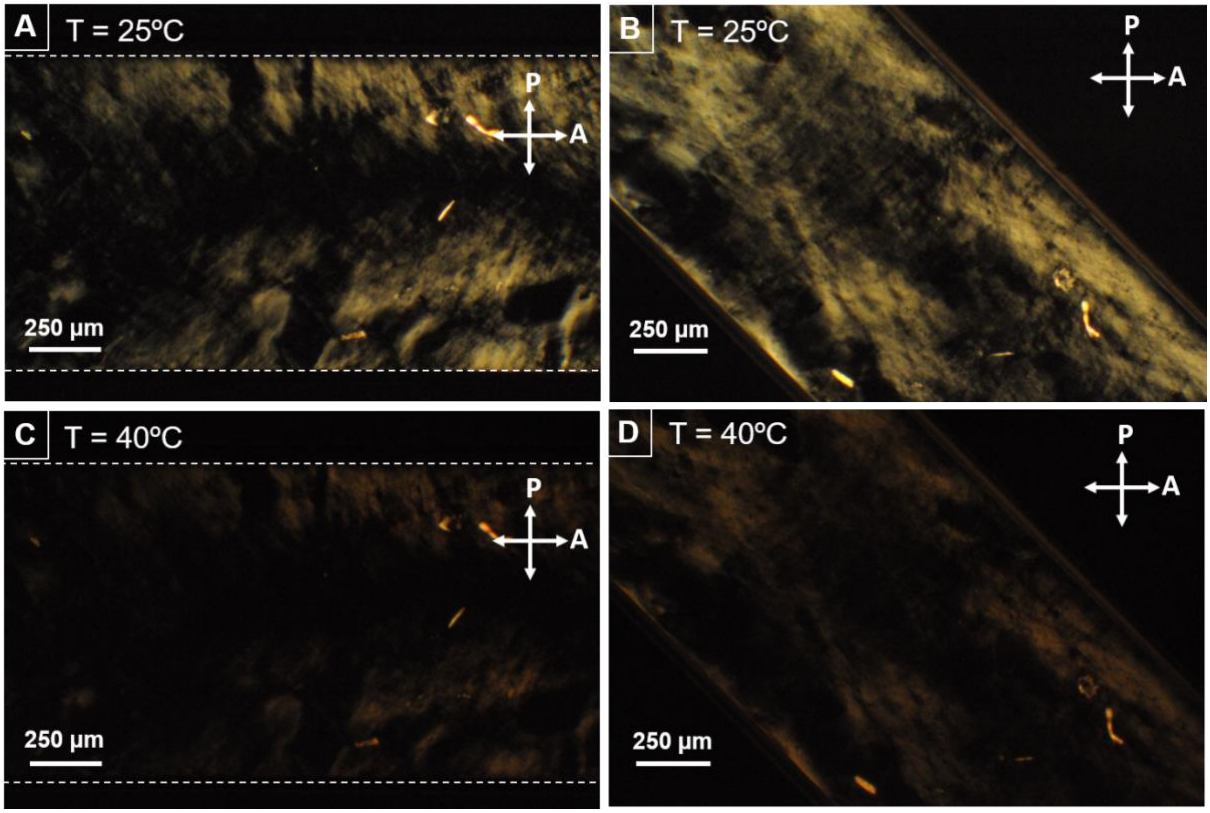


**Figure 5**. (A-D) Polarized optical micrographs of an aqueous suspension of 10 wt% *p*-PNIPAM-*g*-CNCs in a glass capillary. The left (A,C) and right (B,D) columns shows the same sample aligned parallel and in an angle of 45 degrees relative to the analyzer. The top images (A,B) were taken at 25°C, the bottom images (C,D) at 40°C. Dashed white lines indicate the boundary of the capillary.

Keeping the particle concentration the same, a 13 wt% aqueous suspension of *b*-PNIPAM-*g*-CNCs (corresponding to 8.2 wt% CNCs and 4.8 wt% grafted PNIPAM) was prepared and this sample displayed birefringence under crossed polarizers at room temperature (**Figure 6a-b**). However, upon heating, instead of dimming in intensity like the "patchy" CNC dispersion, the birefringence actually became brighter and changed its color (**Figure 6c-d**). This is interpreted to be from the collapse of PNIPAM chains when passing through the LCST; the "brush" CNCs are rendered more hydrophobic so that they phase separate from the water near the walls of the capillary (Figure 6d). The fingerprint texture was not found in this sample and minimal differences in birefringence were observed when rotating the analyzer (**Figure S11**).

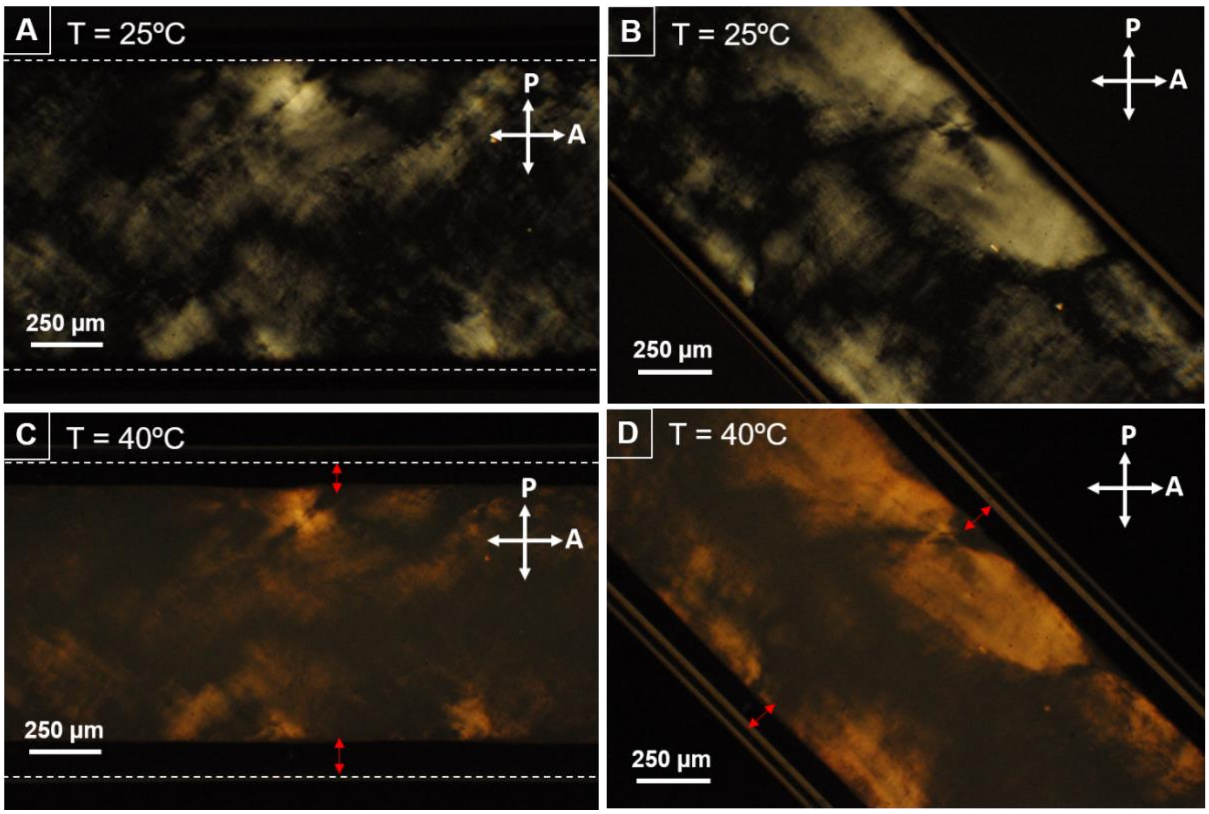


**Figure 6**. (A-D) Polarized optical micrographs of an aqueous suspension of 13 wt% *b*-PNIPAM-*g*-CNCs in a glass capillary. The left (A,C) and right (B,D) columns shows the same sample aligned parallel and in an angle of 45 degrees relative to the analyzer. The top images (A,B) were taken at 25°C, the bottom images (C,D) at 40°C. Red arrows in D indicate an isotropic phase near the capillary walls due to phase separation. Dashed white lines indicate the boundary of the capillary.

To investigate the reversibility of the observed thermal transitions, samples were progressively heated and subsequently cooled at a rate of 1 °C/minute. Images were captured in 1 °C intervals and the intensity of the images was compared to that of the image recorded at room temperature ($I/I_{25°C}$). The intensity of the *p*-PNIPAM-*g*-CNC suspension was nearly constant upon heating to 33 ºC, followed by a stepwise drop at 33-34 °C after which the intensity leveled out at ca. 40% of the original value (**Figure 7**). When the sample was cooled back down to room temperature, the normalized image intensity matched the data acquired upon heating. The plot of the *b*-PNIPAM-*g*-CNC suspension shows an initial decrease of $I/I_{25°}$ but at 33-34 °C a stepwise increased to 135% of the original value is observed. Although the starting and final images at 25 °C have almost identical intensity values, the trace of the *b*-PNIPAM-*g*-CNCs shows a slight hysteresis around the LCST, consistent with the occurrence of phase separation

upon heating and thus a kinetically-delayed response upon cooling. This hysteresis decreased considerably with a slower heating/cooling rate but did not disappear entirely (**Figure S12**). The residual hysteresis may be due to the formation of intrachain hydrogen bonding of the PNIPAM in its collapsed state.[68]

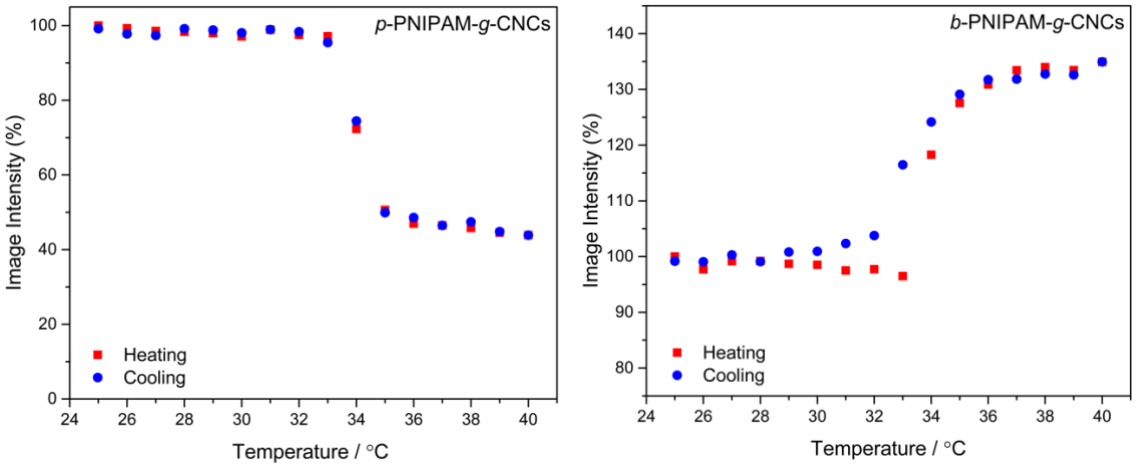


**Figure 7**. Image intensity of polarized optical micrographs of 10 wt% *p*-PNIPAM-*g*-CNCs (left) and 13 wt% b-PNIPAM-*g*-CNCs (right) as a function of temperature during a 1 °C/min heating and cooling cycle.

The drastically different thermal response of the aqueous suspensions of "patchy" and "brush" CNCs is a result of their dissimilar colloidal interactions. The *p*-PNIPAM-*g*-CNCs liquid crystal turned "off" with heat on account of the collapse of the PNIPAM chains, which effectively reduced the packing density of the rods (**Figure 8**). This collapse provides the "patchy" CNCs with increased translational and rotational freedom with minimal attractive interactions, which was observed in the light scattering studies as well (**Figure 4**). The dispersion of the *b*-PNIPAM-*g*-CNCs, by contrast, displays an LC phase through the LCST because the attractive interactions dominate and the rods pack more tightly (**Figure 8**). The higher grafting density of the "brush" PNIPAM-CNCs made the particles more hydrophobic when the PNIPAM collapsed, causing them to attract to one another and expel water in the process. As a result, the LC phase contracted and separated from the walls of the capillary. The increase in intensity was also accompanied by a change in the color. The source of this color

shift is likely due to a change in refractive index of the collapsed PNIPAM compared to its swollen state. As white light traverses the liquid-crystalline sample, it is split into ordinary and extraordinary rays. The degree to which one is retarded compared to the other depends on Δn. When the rays are recombined after the analyzer, some wavelengths may destructively interfere, providing a color change.[69]

To further support these conclusions, controls were prepared consisting of aqueous solutions/suspensions containing free PNIPAM (either 1.8 wt% or 4.8 wt% to match the concentrations of the suspensions of the "patchy" and "brush" CNCs studied) or physical mixtures of PNIPAM and CNCs (1.8 % PNIPAM + 8.2 % CNCs or 4.8 % PNIPAM + 8.2 % CNCs). While the pure PNIPAM solutions did not exhibit any birefringence (**Figure S13**), the mixed PNIPAM + CNC samples clearly exhibited a LC phase (**Figure S14)**, but unlike the grafted PNIPAM-CNC liquid crystals, did not show a significant response to temperature. These results indicate that the covalent attachment of PNIPAM chains at the CNC surface is critical for manipulation of the LC phases with a change in temperature. In the case of mixed PNIPAM + CNC samples, the free PNIPAM chains likely collapse and aggregate with other collapsed chains without affecting the electrostatic repulsions and, thus, the spacing between CNCs. The 1.8 % PNIPAM + 8.2 wt% CNCs sample experienced an 8% decrease in birefringence intensity and the 4.8 % PNIPAM + 8.2 wt% CNCs sample decreased in brightness by 17%.

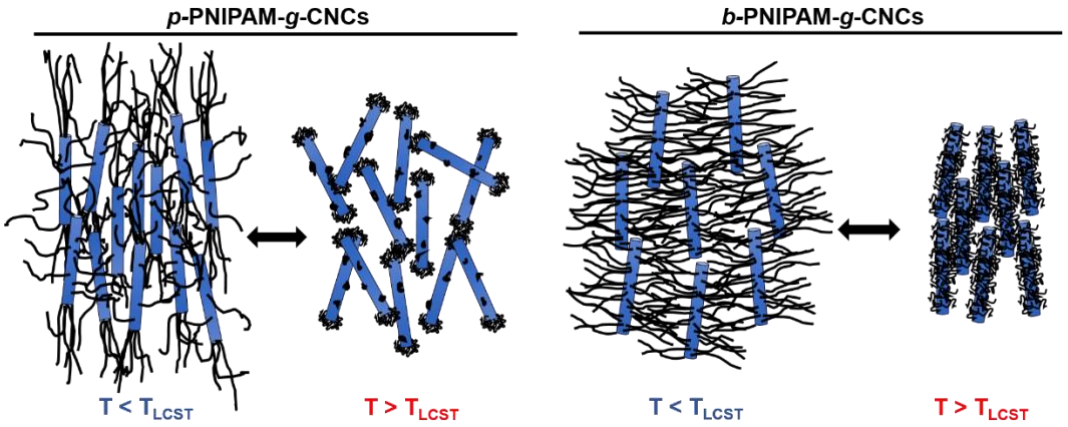


**Figure 8**. Schematic illustrating the proposed temperature-responsive assembly in aqueous dispersions of *p*-PNIPAM-*g*-CNCs and *b*-PNIPAM-*g*-CNCs below and above the LCST of PNIPAM. Not drawn to scale.

## 3. Conclusions

Preferential decoration of CNCs with alkyl bromide initiator groups enabled "patchy" grafting of the thermoresponsive polymer PNIPAM via SI-ATRP. The number of available reducing end groups on CNCs and the subsequent modification steps were successfully quantified by colorimetric assays. These particles were more colloidally stable than their full "brush" counterparts above the LCST of PNIPAM as measured by dynamic light scattering. Both types of modified particles formed LC phases at room temperature, but their responses to heat were different. The loss of birefringence of the "patchy" PNIPAM-CNC liquid crystal caused the light transmittance through crossed polarizers to decrease by 60 % starting at 33 °C whereas the "brush" PNIPAM-CNC liquid crystal increased in brightness by 35 %. The increased brightness was attributed to attractive particle interactions when the solubility of the PNIPAM decreased above its LCST. The "patchy" particles had a lower polymer content and therefore did not exhibit the same response. Rather, the translational and rotational freedom afforded by the collapse of the PNIPAM chains resulted in the liquid crystal switching "off". Pure PNIPAM solutions and PNIPAM + CNC physical blends were prepared as controls. No birefringence was observed in the pure PNIPAM solutions and the birefringence that was observed in the PNIPAM + CNC blends did not change with temperature. Therefore, chemical grafting of

PNIPAM in a "patchy" morphology proved to be the optimal method for developing a liquid crystal temperature "switch". This system could be used to template materials that have an electric or colorimetric response to aggregation, providing a basis for a thermal sensor. Furthermore, the temperature range for the response can be adjusted based on the monomer(s) chosen in the polymerization. For example, the liquid crystal switch could be tailored within 25-90 °C by using this reaction scheme to graft poly(ethylene glycol) methacrylates with varying ethylene glycol side chain lengths.[32, 34, 70] Effects of the grafted polymer molecular weight and concentration of particles on the temperature response of the liquid crystal are likely to be fruitful subjects for future studies.

## 4. Experimental Section

*Materials:* CNCs derived from wood pulp were obtained from the USDA Forest Products Laboratory (purchased from the University of Maine) in aqueous slurry form (13.5 wt%). A 1 wt% suspension at RT has a pH of 6.8 and a conductivity of 81.3 µS/cm. This suspension was subsequently diluted to the desired concentrations for the following reactions and the concentration of reaction products was determined gravimetrically. 2-Bromoisobutanoic acid *N*-hydroxysuccinimide ester (NHS-BiB), *N*-(3-dimethylaminopropyl)-N'-ethylcarbodiimide hydrochloride (EDC-HCl), ethylenediamine (EDA), *N*-isopropylacrylamide (NIPAM, 97 %), copper (I) chloride, copper (II) bromide, *N,N,N',N'',N*''-pentamethyldiethylenetriamine (PMDETA), acetic acid (glacial, 100%), aqueous hydrochloric acid (37 %), dimethyl sulfoxide (99.5 %), methanol (99 %), sodium chlorite ($NaClO_2$), sodium phosphate dibasic ($Na_2HPO_4$), sodium hydroxide pellets, *p*-toluenesulfonic acid (12 % in acetic acid), 2-bromopropionic acid, poly(*N*-isopropylacrylamide) (PNIPAM, $M_n$ = 30,000 Da), and dialysis tubing cellulose membrane (MWCO 7 kDa) were all purchased from Sigma-Aldrich. The NIPAM was purified by recrystallization from 60:40 toluene:hexanes (v/v) prior to use. All other chemicals were

used without further purification. Borosilicate glass rectangular capillaries of dimensions 0.1 x 1.0 x 50 $mm^3$ were purchased from VitroCom Inc. and used without surface treatment. Millipore-processed (Darmstadt, Germany) deionized (DI) water was used with a resistivity of 18.2 MΩ-cm.

*"Patchy" Initiator Decoration*

Oxidation of Reducing Aldehyde End Groups: 100 mL of a 1 wt% aqueous CNC suspension was stirred in a 250 mL round bottom flask. $NaClO_2$ (2.83 g) was added to the CNC suspension to obtain a 313 mM solution. The reaction mixture was stirred for 30 min before the pH was adjusted to 3.5 with acetic acid. The mixture was stirred for 20 hours at room temperature (21-22 ºC). The CNCs were subsequently dialyzed until a dialysate pH of 6-7 was reached and were afterwards kept as an aqueous suspension.

Amination of -COOH Groups: 100 mL of the oxidized CNCs (previously dialyzed, 1 wt%) were placed into a 250 mL round bottom flask and the suspension was magnetically stirred. $Na_2HPO_4$ (0.71 g) was added to the CNC suspension to obtain a 50 mM solution. The pH was adjusted to 6.5 with NaOH or HCl, followed by the addition of 20 μL (0.3 mmol) of EDA. Finally, EDC-HCl (0.1 g) was added and the mixture was stirred for 4 hours at room temperature (21-22 ºC). The CNCs were dialyzed against deionized water and afterwards kept as an aqueous suspension.

Attachment of ATRP Initiator to Amine Functionality: 100 mL of amine-functionalized CNCs (previously dialyzed, 1 wt%) were added to a 250 mL round bottom flask and the suspension was magnetically stirred. $Na_2HPO_4$ (0.14 g) was added to the CNC suspension to obtain a 10 mM solution. The pH was adjusted to 7.2 with NaOH or HCl. In a separate vial, NHS-BiB (87 mg) was dissolved in 10 mL of DMSO and the solution was added dropwise to the flask containing the amine end-functionalized CNCs. The mixture was left to react for 4 hours at

room temperature (21-22 ºC), followed by dialysis against deionized water. The aqueous suspension of the initiator-modified CNCs thus made was stored at 4 °C. The concentration of the final suspension was determined gravimetrically.

*"Brush" Initiator Decoration:* In a 100 mL round bottom flask, *p*-toluenesulfonic acid (0.28 g, 12 % in acetic acid) was added to 7.4 g of a CNC aqueous slurry (13.5 wt%) and the suspension was magnetically stirred. Next, 2-bromopropionic acid (38.16 mL) was added to the mixture, a condenser was attached to the flask, and the reaction was stirred at 105 °C for 4 hours. The mixture was allowed to cool to room temperature and diluted with DI water so that the CNC content was 1 wt% before transferring to a dialysis membrane. The CNCs were dialyzed against DI water until a dialysate pH of 6-7 was reached. The aqueous suspension thus made was stored at 4 °C. The concentration of the final suspension was determined gravimetrically.

*SI-ATRP:* Polymerizations were carried out with a NIPAM/CuCl/$CuBr_2$/PMDETA molar ratio of 100:1:0.3:2 in $H_2O$/MeOH (50/50 v/v). An aqueous dispersion containing 100 mg of the initiator-modified CNCs was placed in a 250 mL round bottom flask. DI water (to bring the total water volume to 50 mL) and 50 mL of methanol were added. Then, 10 g of recrystallized NIPAM, 360 uL PMDETA, and 58 mg of $CuBr_2$ were added to the flask with a stir bar and the flask was sealed with a septum. The mixture was subjected to three freeze-pump-thaw cycles with magnetic stirring. Finally, 88 mg of CuCl were added under a nitrogen blanket (positive pressure in flask) to initiate the polymerization and the flask was resealed. The mixture was stirred for 2 hours at ambient temperature before being subjected to dialysis against deionized water until neutral pH was reached. The aqueous suspension was stored at 4 °C; aliquots taken from this batch were freeze-dried for analysis.

*Cleavage of PNIPAM Brushes via Hydrolysis:* Approximately 100 mg of PNIPAM-grafted-CNCs were suspended in 20 mL of aqueous 2 wt% NaOH and the mixture was stirred at ambient temperature for 72 hours, before the CNCs were separated off by centrifugation at 9000 rpm for 15 min. The supernatant was collected, neutralized to pH 7 with HCl, and dialyzed against DI water (3500 Da MWCO). The polymers were oven dried and dissolved in DMF for analysis.

*Size Exclusion Chromatography (SEC)*: a SEC-MALS setup was used to determine the molecular weights and polydispersities of cleaved PNIPAM samples. The SEC system consisted of a Tosoh EcoSEC. The mobile phase was 0.1 M LiBr in DMF. The MALS system consisted of a Wyatt Dawn EOS and a Wyatt REX differential refractive index detector (DRI). Analysis was completed using Astra 5.3 software. The reported chromatograms displayed the light scattering trace from the 90º detector. The dndc value for PNIPAM used was 0.071 mL/g.[71]

*Bicinchoninic Acid Assay:* This assay was adapted from a literature procedure.[72] Two solutions were prepared: Solution A (pH 9.7), contained 5.428 g of $Na_2CO_3$, 2.42 g of $NaHCO_3$, and 0.1942 g of BCA disodium salt hydrate in 100 mL of Milli-Q water. Solution B contained 0.1248 g of $CuSO_4 \cdot 5\ H_2O$ and 0.1262 g of L-serine in 100 mL of Milli-Q water.

Preparation of the calibration curve (**Figure S15**). A calibration curve was obtained with 0 – 8 x $10^{-5}$ M glucose solutions. For each concentration in the calibration curve, 2 mL of glucose solution, 1 mL of Solution A, and 1 mL of Solution B were added to a glass vial. Each vial was sealed and shaken by hand prior to heating to 75 °C for 30 min in a water bath. The vials were cooled to RT and their absorbance was measured at 560 nm.

Reducing end quantification. The same procedure was performed as for the calibration curve except that the 2 mL of glucose solution was replaced by 2 mL of a CNC suspension containing

5.0 x $10^{-3}$ g of CNCs (0.25 wt%). Once the suspensions were at room temperature after the heating step, they were centrifuged at 9000 rpm for 4 min. The absorbance of the supernatant was measured at 560 nm. The experiments were done in triplicate.

*Ninhydrin Assay:* The procedure was adapted from a literature procedure.[55]

Preparation of the calibration curve (**Figure S16**). A calibration curve was obtained using 2-ethyl-1-hexylamine in DI water with concentrations ranging from $10^{-5}$ M to 2.5 x $10^{-4}$ M. 2 mL of the 2-ethyl-1-hexylamine and 1 mL of the ninhydrin reagent solution (ninhydrin and hydrinatin with lithium acetate buffer, pH 5.2) were added to a microwave vial sealed under $N_2$, shaken by hand and heated for 30 min at 100 °C. The tubes were then cooled down to room temperature and 5 mL of 50 % (v/v) ethanol/water was added to the mixture. 15 seconds of stirring using a Vortex mixer was performed in order to oxidize the excess of hydrindantin in the solution. The absorbance was recorded at 570 nm.

Ninhydrin test on samples. 2 mL of a 0.5 wt% CNC suspension were used for the quantification of the primary amines. The same procedure was followed for the different samples of the calibration curve except that after vortex mixing, the CNCs were removed from the suspension by centrifugation (9000 rpm, 4 min). The absorbance of the supernatants was measured at 570 nm. The experiments were done in triplicate.

*Wide angle X-ray Diffraction.* The WAXS spectra was recorded with an S-MAX3000 pinhole camera (Rigaku Innovative Technologies, Auburn Hills, USA). The CNC film was kept under vacuum at room temperature during the measurement. Raw data was processed according to a standard procedure (Figure S2).

*Conductometric Titration.* Conductometric titration was performed with a S47 SevenMulti™ dual meter pH / conductivity probe. Prior to conductometric titration, the suspension was passed

through a strong acid cation (SAC) exchange resin column. Then, 9 mL of a 0.796 wt% CNC suspension containing 1 mM NaCl was titrated against 9.89 mM NaOH solution. The first equivalence point indicates the sulfate half ester groups (312 µmol $–OSO_3$/g CNCs), the second equivalence point indicates the carboxylic acid groups (26 µmol –COOH/g CNCs) (Figure S3).

*Atomic Force Microscopy (AFM).* Freshly cleaved mica was functionalized with poly-L-lysine aqueous solution by drop-casting 40 µL onto the mica, it was washed off with milli-Q water and dried under a nitrogen flow. CNCs suspensions (0.001 – 0.005 wt%, 30 µL) were spin-coated onto the functionalized mica at 2000 rpm and subsequently washed with milli-Q water and dried under nitrogen flow. The images were acquired with a JPK NanoWizard II, in tapping mode with PPP-NCSTR probes at room temperature.

*IR Spectroscopy.* Freeze-dried CNC samples were analyzed by a Thermo Scientific Nicolet iS50 Fourier-transform infrared (FTIR) spectrometer in in attenuated total reflectance (ATR) mode.

*Thermogravimetric Analysis (TGA).* Thermograms of freeze-dried CNC samples were measured with an SDT Q600 (TA Instruments) in ramp mode from 30 °C to 600 °C at 10 °C/min.

*Elemental Analysis.* Bromine content (wt %) was determined by flask combustion followed by ion chromatography and was performed by Atlantic Microlab, Inc.

*Polarized Optical Microscopy (POM).* POM images of the filled capillaries (0.1 x 1.0 mm ID) were taken using a Leica DMRX optical microscope equipped with rotatable polarizer and analyzer, and a Nikon D300 digital SLR camera.

*Zeta Potential*. A Malvern Zetasizer Nano Z system ($\lambda$ = 632.8 nm) was used to analyze the electrophoretic mobility of the aqueous CNC dispersions (0.1 wt%) at 25 °C and 40 °C. Electrophoretic mobility was converted to zeta potential through the Smoluchowski model. No salt was added to the samples prior to analysis and all of the samples had a pH of 8.1 ± 0.1.

*Multi-Angle Dynamic Light Scattering (MADLS).* Particle size was measured using a custom-built multi-angle light scattering apparatus equipped with a 660 nm laser source and an ALV-5000/E digital autocorrelator. Approximately 5 mL of each 0.1 wt% aqueous CNC suspension was transferred into a dust-free vial using a syringe attached to a 0.22 um Millipore PDVF membrane filter. Runs were performed for each sample and temperature at five scattering angles (30 °, 45 °, 60 °, 75 °, 90 °). The average apparent hydrodynamic radius was calculated from a third order cumulant fitting of the intensity autocorrelation function, extrapolated to zero scattering angle.

**Supporting Information**

Supporting Information is available from the Wiley Online Library or from the author.

**Acknowledgements**

Financial support from the ThinkSwiss scholarship hosted by Dr. Alke Fink and the Georgia Institute of Technology Renewable Bioproducts Institute is gratefully acknowledged. B.R. is thankful for support from the Center for the Science and Technology of Advanced Materials and Interfaces (STAMI) graduate fellowship program at Georgia Tech. J.Z. and G.D. acknowledge financial support from the Swiss National Science Foundation (Ambizione Grant no. PZ00P2_167900). C.W. acknowledges financial support through the Army Research Office under Grant No. W911NF-15-1-0190 and the Adolphe Merkle Foundation. E.R., B.R. and P.R.

appreciate support from the National Science Foundation Division of Materials Research (Award no. 1609058). The authors are thankful for Paul Balding's assistance with size exclusion chromatography.

Received: ((will be filled in by the editorial staff))
Revised: ((will be filled in by the editorial staff))
Published online: ((will be filled in by the editorial staff))

**References**


1. T. Uchida, *Japanese Journal of Applied Physics* **2014**, *53*.
2. T. Larsen, A. Bjarklev, D. Hermann, J. Broeng, *Opt. Express* **2003**, *11*.
3. J. Hwang, M.H. Song, B. Park, S. Nishimura, T. Toyooka, J.W. Wu, Y. Takanishi, K. Ishikawa, H. Takezoe, *Nat Mater* **2005**, *4*, 383.
4. M. Ozaki, M. Kasano, T. Kitasho, D. Ganzke, W. Haase, K. Yoshino, *Adv. Mater.* **2003**, *15*, 974.
5. H. Coles,S. Morris, *Nature Photonics* **2010**, *4*, 676.
6. S. Chandrasekhar, *Liquid Crystals*. Cambridge University Press, **1992**.
7. A. Querejeta-Fernandez, B. Kopera, K.S. Prado, A. Klinkova, M. Methot, G. Chauve, J. Bouchard, A.S. Helmy, E. Kumacheva, *ACS Nano* **2015**, *9*, 10377.
8. G. Chu, X. Wang, H. Yin, Y. Shi, H. Jiang, T. Chen, J. Gao, D. Qu, Y. Xu, D. Ding, *ACS Appl Mater Interfaces* **2015**, *7*, 21797.
9. R.-Y. Wang, H. Wang, X. Wu, Y. Ji, P. Wang, Y. Qu, T.-S. Chung, *Soft Matter* **2011**, *7*, 8370.
10. E. Dujardin, M. Blaseby, S. Mann, *J. Mater. Chem.* **2003**, *13*, 696.
11. T.D. Nguyen, K.E. Shopsowitz, M.J. MacLachlan, *Chemistry* **2013**, *19*, 15148.
12. K.E. Shopsowitz, J.A. Kelly, W.Y. Hamad, M.J. MacLachlan, *Adv. Funct. Mater.* **2014**, *24*, 327.
13. P. van der Asdonk, M. Keshavarz, P.C. Christianen, P.H. Kouwer, *Soft Matter* **2016**, *12*, 6518.
14. P. van der Asdonk, H.C. Hendrikse, M. Fernandez-Castano Romera, D. Voerman, B.E.I. Ramakers, D.W.P.M. Löwik, R.P. Sijbesma, P.H.J. Kouwer, *Adv. Funct. Mater.* **2016**, *26*, 2609.
15. P. van der Asdonk,P.H.J. Kouwer, *Chem. Soc. Rev.* **2017**, *46*, 5935.
16. G.R. Meseck, A.S. Terpstra, M.J. MacLachlan, *Current Opinion in Colloid & Interface Science* **2017**, *29*, 9.
17. S. Camarero-Espinosa, C. Endes, S. Mueller, A. Petri-Fink, B. Rothen-Rutishauser, C. Weder, M. Clift, E. Foster, *Fibers* **2016**, *4*.
18. C. Endes, S. Camarero-Espinosa, S. Mueller, E.J. Foster, A. Petri-Fink, B. Rothen-Rutishauser, C. Weder, M.J. Clift, *J Nanobiotechnology* **2016**, *14*, 78.
19. M. Giese, L.K. Blusch, M.K. Khan, M.J. MacLachlan, *Angew. Chem. Int. Ed. Engl.* **2015**, *54*, 2888.
20. E. Belamie,M.M. Giraud-Guille, *Liquid-crystalline behavior in aqueous suspensions of elongated chitin microcrystals*. Trends in Colloid and Interface Science XVII. Springer, Berlin, Heidelberg **2004**.
21. J.F. Revol,R.H. Marchessault, *International Journal of Biological Macromolecules* **1993**, *15*, 329.
22. T.T.L. Chau, D.Q.T. Le, H.T. Le, C.D. Nguyen, L.V. Nguyen, T.D. Nguyen, *ACS Appl Mater Interfaces* **2017**, *9*, 30812.
23. J.A. Kelly, M. Giese, K.E. Shopsowitz, W.Y. Hamad, M.J. MacLachlan, *Acc. Chem. Res.* **2014**, *47*, 1088.
24. A. Hirai, O. Inui, F. Horii, M. Tsuji, *Langmuir* **2009**, *25*, 497.
25. B.E. Risteen, A. Blake, M.A. McBride, C. Rosu, J.O. Park, M. Srinivasarao, P.S. Russo, E. Reichmanis, *Biomacromolecules* **2017**, *18*, 1556.
26. M.A. Stuart, W.T. Huck, J. Genzer, M. Muller, C. Ober, M. Stamm, G.B. Sukhorukov, I. Szleifer, V.V. Tsukruk, M. Urban, F. Winnik, S. Zauscher, I. Luzinov, S. Minko, *Nat Mater* **2010**, *9*, 101.

27. S. Wohlhauser, G. Delepierre, M. Labet, G. Morandi, W. Thielemans, C. Weder, J.O. Zoppe, *Macromolecules* **2018**, *Submitted*.
28. U.D. Hemraz, A. Lu, R. Sunasee, Y. Boluk, *J. Colloid Interface Sci.* **2014**, *430*, 157.
29. J.O. Zoppe, Y. Habibi, O.J. Rojas, R.A. Venditti, L.S. Johansson, K. Efimenko, M. Osterberg, J. Laine, *Biomacromolecules* **2010**, *11*, 2683.
30. E. Zeinali, V. Haddadi-Asl, H. Roghani-Mamaqani, *RSC Adv.* **2014**, *4*, 31428.
31. M. Haqani, H. Roghani-Mamaqani, M. Salami-Kalajahi, *Cellulose* **2017**, *24*, 2241.
32. X. Zhang, J. Zhang, L. Dong, S. Ren, Q. Wu, T. Lei, *Cellulose* **2017**, *24*, 4189.
33. J.O. Zoppe, M. Osterberg, R.A. Venditti, J. Laine, O.J. Rojas, *Biomacromolecules* **2011**, *12*, 2788.
34. N. Grishkewich, S.P. Akhlaghi, Y. Zhaoling, R. Berry, K.C. Tam, *Carbohydr. Polym.* **2016**, *144*, 215.
35. J. Zhang, Q. Wu, M.-C. Li, K. Song, X. Sun, S.-Y. Lee, T. Lei, *ACS Sustainable Chemistry & Engineering* **2017**, *5*, 7439.
36. W. Wu, F. Huang, S. Pan, W. Mu, X. Meng, H. Yang, Z. Xu, A.J. Ragauskas, Y. Deng, *J. Mater. Chem. A* **2015**, *3*, 1995.
37. F. Azzam, E. Siqueira, S. Fort, R. Hassaini, F. Pignon, C. Travelet, J.L. Putaux, B. Jean, *Biomacromolecules* **2016**, *17*, 2112.
38. F. Azzam, L. Heux, J.L. Putaux, B. Jean, *Biomacromolecules* **2010**, *11*, 3652.
39. J.O. Zoppe, R.A. Venditti, O.J. Rojas, *J. Colloid Interface Sci.* **2012**, *369*, 202.
40. W. Wu, J. Li, W. Liu, Y. Deng, *BioResources* **2016**, *11*.
41. J. Yi, Q. Xu, X. Zhang, H. Zhang, *Cellulose* **2009**, *16*, 989.
42. R.J. Moon, A. Martini, J. Nairn, J. Simonsen, J. Youngblood, *Chem. Soc. Rev.* **2011**, *40*, 3941.
43. A.R. Lokanathan, A. Nykanen, J. Seitsonen, L.S. Johansson, J. Campbell, O.J. Rojas, O. Ikkala, J. Laine, *Biomacromolecules* **2013**, *14*, 2807.
44. L.R. Arcot, M. Lundahl, O.J. Rojas, J. Laine, *Cellulose* **2014**, *21*, 4209.
45. M.A. Karaaslan, G. Gao, J.F. Kadla, *Cellulose* **2013**, *20*, 2655.
46. J.O. Zoppe, A.V.M. Dupire, T.G.G. Lachat, P. Lemal, L. Rodriguez-Lorenzo, A. Petri-Fink, C. Weder, H.-A. Klok, *ACS Macro Letters* **2017**, 892.
47. E. Sipahi-Saglam, M. Gelbrich, E. Gruber, *Cellulose* **2003**, *10*, 237.
48. Y. Habibi, L.A. Lucia, O.J. Rojas, *Chem. Rev.* **2010**, *110*, 3479.
49. M. Heskins,J.E. Guillet, *Journal of Macromolecular Science: Part A - Chemistry* **1968**, *2*, 1441.
50. E.J. Foster, R.J. Moon, U.P. Agarwal, M.J. Bortner, J. Bras, S. Camarero-Espinosa, K.J. Chan, M.J.D. Clift, E.D. Cranston, S.J. Eichhorn, D.M. Fox, W.Y. Hamad, L. Heux, B. Jean, M. Korey, W. Nieh, K.J. Ong, M.S. Reid, S. Renneckar, R. Roberts, J.A. Shatkin, J. Simonsen, K. Stinson-Bagby, N. Wanasekara, J. Youngblood, *Chem. Soc. Rev.* **2018**, *47*, 2609.
51. A.C. OSullivan, *Cellulose* **1997**, *4*, 173.
52. M.S. Reid, M. Villalobos, E.D. Cranston, *Langmuir* **2016**.
53. K. Mopper,E.M. Gindler, *Anal. Biochem.* **1973**, *56*, 440.
54. P.K. Smith, R.I. Krohn, G.T. Hermanson, A.K. Mallia, F.H. Gartner, M.D. Provenzano, E.K. Fujimoto, N.M. Goeke, B.J. Olson, D.C. Klenk, *Anal. Biochem.* **1985**, *150*, 76.
55. S. Prochazkova, K.M. Vårum, K. Ostgaard, *Carbohydr. Polym.* **1999**, *38*, 115.
56. E. Kaiser, R.L. Colescott, C.D. Bossinger, P.I. Cook, *Anal. Biochem.* **1970**, *34*, 595.
57. E. Poli, V. Chaleix, C. Damia, Z. Hjezi, E. Champion, V. Sol, *Anal. Methods* **2014**, *6*, 9622.

58. S. Beck, M. Méthot, J. Bouchard, *Cellulose* **2014**, *22*, 101.
59. L. Du, J. Wang, Y. Zhang, C. Qi, M.P. Wolcott, Z. Yu, *Nanomaterials (Basel)* **2017**, *7*.
60. Y. Habibi, H. Chanzy, M.R. Vignon, *Cellulose* **2006**, *13*, 679.
61. G. Morandi, L. Heath, W. Thielemans, *Langmuir* **2009**, *25*, 8280.
62. J.O. Zoppe, N.C. Ataman, P. Mocny, J. Wang, J. Moraes, H.A. Klok, *Chem. Rev.* **2017**, *117*, 1105.
63. J.O. Zoppe, M.S. Peresin, Y. Habibi, R.A. Venditti, O.J. Rojas, *ACS Appl Mater Interfaces* **2009**, *1*, 1996.
64. R.E. Behling, B.A. Williams, B.L. Staade, L.M. Wolf, E.W. Cochran, *Macromolecules* **2009**, *42*, 1867.
65. J.P.F. Lagerwall, C. Schütz, M. Salajkova, J. Noh, J. Hyun Park, G. Scalia, L. Bergström, *NPG Asia Materials* **2014**, *6*, e80.
66. J. Majoinen, J. Hassinen, J.S. Haataja, H.T. Rekola, E. Kontturi, M.A. Kostiainen, R.H. Ras, P. Torma, O. Ikkala, *Adv. Mater.* **2016**, *28*, 5262.
67. T. Abitbol, D. Kam, Y. Levi-Kalisman, D.G. Gray, O. Shoseyov, *Langmuir* **2018**, *34*, 3925.
68. X. Wang, X. Qiu, C. Wu, *Macromolecules* **1998**, *31*, 2972.
69. A. Sommerfeld, *Optics*. Lectures on Theoretical Physics. Vol. 4. Academic Press, **1964**.
70. C. Porsch, S. Hansson, N. Nordgren, E. Malmström, *Polymer Chemistry* **2011**, *2*, 1114.
71. U. Nobbmann. *The Chromatogram Series: PNIPAm*. Materials Talks 2014; Available from: http://www.materials-talks.com/blog/2014/01/16/the-chromatogram-series-pnipam/.
72. Y.H. Zhang,L.R. Lynd, *Biomacromolecules* **2005**, *6*, 1510.

**TOC Entry**

A temperature-switchable bio-derived liquid crystal is developed by “patchy” functionalization of cellulose nanocrystals with the thermoresponsive polymer poly(N-isopropylacrylamide) (PNIPAM) and forming aqueous suspensions. The liquid crystal is “on” at room temperature but turns “off” above the LCST of PNIPAM when the polymer chains collapse onto the rods and reduce the packing density of the particles.

**Keyword:** thermoresponsive liquid crystal

B. Risteen, G. Delepierre, M. Srinivasarao, C. Weder, P. Russo, E. Reichmanis, J, Zoppe*

**Thermally switchable liquid crystals based on cellulose nanocrystals with patchy polymer grafts**